Analysis of longitudinal cracked two-dimensional functionally graded beams exhibiting material non-linearity

Victor Rizov
Department of Technical Mechanics, University of Architecture, Civil Engineering and Geodesy, 1 Chr. Smirnensky blvd., 1046 – Sofia, Bulgaria.
v_rizov_fhe@uacg.bg

ABSTRACT. An analytical study of longitudinal fracture in two-dimensional functionally graded cantilever beam configurations is carried-out with taking into account the non-linear behavior of material. A longitudinal crack is located arbitrary along the beam cross-section height. The material is functionally graded along the width as well as along the height of beam. The external loading consists of a bending moment applied at the free end of lower crack arm. Fracture is studied in terms of the strain energy release rate by considering the beam complementary strain energy. The solution derived is verified by analyzing the longitudinal crack with the help of the *J*-integral. The distribution of *J*-integral value along the crack front is studied. The effects of crack location, material gradients and non-linear behavior of material on the fracture are elucidated. The analysis reveals that the material non-linearity has to be taken into account in fracture mechanics based safety design of structural members and components made of two-dimensional functionally graded materials.

KEYWORDS. Functionally graded beam; Crack; Material non-linearity; Analytical solution.

Citation: Rizov, V., Analysis of longitudinal cracked two-dimensional functionally graded beams exhibiting material non-linearity, Frattura ed Integrità Strutturale, 41 (2017) 491-503.

Received: 23.04.2017
Accepted: 28.05.2017
Published: 01.07.2017

INTRODUCTION

The functionally graded materials are new inhomogeneous materials produced by mixing of two constituent materials in different proportions in order to satisfy the requirements of material properties in different parts of a structural member [1-12]. Since the composition of constituent materials varies continuously along one or more spatial coordinates during manufacturing without sudden changes of material properties, the interfaces and stress concentrations are largely avoided in contrast to laminated composite materials [13-15]. Besides, the performance of functionally graded structural members and components to the external load can be optimized by tailoring the variation of material properties in a desired way during manufacturing. Therefore, the functionally graded materials have been widely applied as advanced structural materials in aeronautics, electronics, nuclear energy, optics, engineering and biomedicine for

the last three decades [16]. Fracture behavior is crucial for structural integrity and functionality of members and components made of functionally graded materials. Therefore, considerable attention has been paid to fracture in these novel materials by the international research community [17-22].
The present paper is concerned with a longitudinal fracture analysis of a two-dimensional functionally graded cantilever beam configuration with taking into account the non-linear behavior of material. Fracture is analyzed in terms of the strain energy release rate. The material is functionally graded along the height as well as along width of the beam. The mechanical behavior of material is described by a power-law stress-strain relation. An additional fracture analysis is carried-out by applying the *J*-integral approach and the results obtained are compared with the strain energy release rate. The effects of material gradients, crack location and material non-linearity on the fracture behavior are elucidated.

ANALYSIS OF THE STRAIN ENERGY RELEASE RATE

The present paper analyses the longitudinal fracture in the two-dimensional functionally graded cantilever beam configuration shown schematically in Fig. 1.

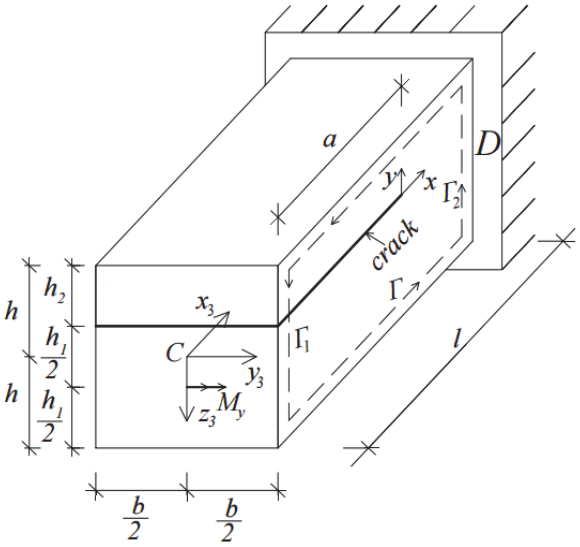

Figure 1: The geometry and loading of the two-dimensional functionally graded cantilever beam.

A longitudinal crack of length, *a*, is located arbitrary along the beam cross-section height (it should be mentioned that the present paper is motivated also by the fact that functionally graded materials can be built up layer by layer [16] which is a premise for appearance of longitudinal cracks between layers). The lower and upper crack arms have different thicknesses denoted by h_1 and h_2, respectively. The beam is loaded by one bending moment, M_y, applied at the free end of lower crack arm (Fig. 1). Thus, the upper crack arm is free of stresses. The beam has a rectangular cross-section of width, *b*, and height, 2*h*. The beam is clamped in section, *D*.
The beam non-linear mechanical behavior is described by the following power-law stress-strain relation [23]:

$$\sigma = B\varepsilon^m \tag{1}$$

where σ is the longitudinal normal stress, ε is the longitudinal strain, *B* and *m* are material properties.
Zircona-titanium is one of the functionally graded materials which exhibit non-linear mechanical behavior. Data for mechanical properties of zircona-titanium can be found in [24].
The material is functionally graded along the width as well as along the height of the beam (Fig. 1). The distribution of material property, *B*, in the beam cross-section is expressed as a function of y_3 and z_3 by the following quadratic law:

$$B = B_0 + \frac{4\,y_3^2}{b^2}B_1 + \frac{z_3^2}{b^2}B_2, \tag{2}$$

where

$$-\frac{b}{2} \le y_3 \le \frac{b}{2},\ -h \le z_3 \le h. \tag{3}$$

In (2), B_0 is the value of B in the centre of the beam cross-section, B_1 and B_2 are material properties which govern the material gradients along axes, y_3 and z_3, respectively (Fig. 1).

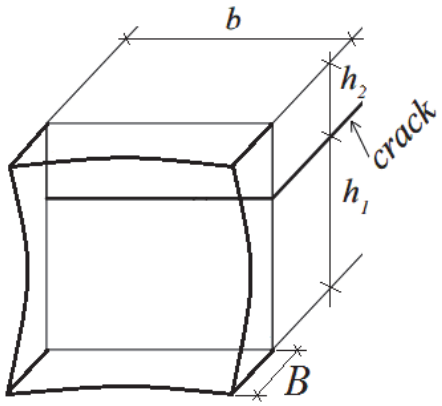

Figure 2: Distribution of the material property, B, in the beam cross-section.

It should be mentioned that Eq. (2) is suitable for two-dimensional functionally graded beam configurations which have high mechanical properties at the lower, upper and lateral surfaces of the beam as shown in Fig. 2.
The fracture behavior is studied in terms of the strain energy release rate. For this purpose, an elementary increase, da, of the crack length is assumed (the external load is kept constant). The strain energy release rate, G, is expressed via the changes of external work, dW_{ext}, and strain energy, dU, as

$$G = \frac{dW_{ext} - dU}{dA} \tag{4}$$

where the increase of crack area is

$$dA = bda \tag{5}$$

The change of external work is written as

$$dW_{ext} = dU + dU^* \tag{6}$$

where dU^* is the change of complementary strain energy.
By combining of (4), (5) and (6), the strain energy release rate can be expressed as

$$G = \frac{dU^*}{bda} \tag{7}$$

It should be noted that the present analysis holds for non-linear elastic behavior of material. The analysis is applicable also for elastic-plastic behavior of material if the beam considered undergoes active deformation, i.e. if the external loading increases only [25]. It should also be mention that the present study is based on the small strains assumption.

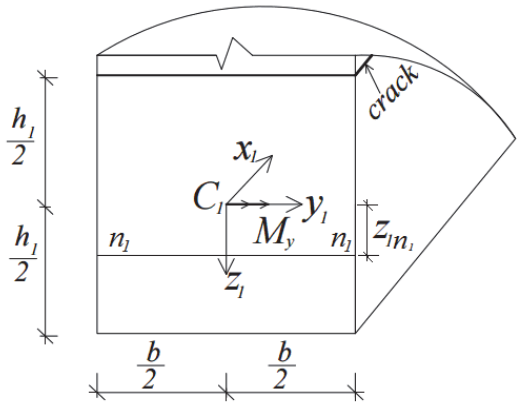

Figure 3: The free end of the lower crack arm (. $n_1 - n_1$. is the neutral axis).

The beam complementary strain energy, U^*, is written as

$$U^* = a\int_{-\frac{h_1}{2}}^{\frac{h_1}{2}}\left(\int_{-\frac{b}{2}}^{\frac{b}{2}} u_{0L}^* dy_1\right)dz_1 + (l-a)\int_{-h}^{h}\left(\int_{-\frac{b}{2}}^{\frac{b}{2}} u_{0U}^* dy_2\right)dz_2 \tag{8}$$

where u_{0L}^* and u_{0U}^* are the complementary strain energy densities in the lower crack arm and the un-cracked beam portion $(a \le x_3 \le l)$, respectively. Axes, y_1 and z_1, are shown in Fig. 3, y_2 and z_2 are the centroidal axes of the cross-section of the un-cracked beam portion.

In principle, the complementary strain energy density is equal to the area *OQR* that supplements the area *OPQ*, enclosed by the stress-strain curve, to a rectangle (Fig. 4). Therefore, the complementary strain energy density in the lower crack arm is written as

$$u_{0L}^* = \sigma\varepsilon - u_{0L} \tag{9}$$

where the strain energy density, u_{0L}, is equal to the area *OPQ*

$$u_{0L} = \int_0^{\varepsilon} \sigma(\varepsilon)d\varepsilon \tag{10}$$

From (1), (9) and (10), the complementary strain energy density can be obtained as

$$u_{0L}^* = B\frac{m\varepsilon^{m+1}}{m+1} \tag{11}$$

The strain distribution is analyzed by applying the Bernoulli's hypothesis for plane sections since the span to height ratio of the beam under consideration is large. Concerning the application of the Bernoulli's hypothesis in the present study, it should also be noted that since the beam is loaded in pure bending (Fig. 1) the only non-zero strain is the longitudinal strain, ε. Therefore, according to the small strain compatibility equations, ε is distributed linearly along the height of the beam cross-section. Thus, ε in the lower crack arm is written as

$$\varepsilon = \left(z_1 - z_{1n_1}\right)\kappa_1 \tag{12}$$

where z_{1n_1} is the coordinate of the neutral axis, $n_1 - n_1$, (the neutral axis shifts from the centroid since the material is functionally graded (Fig. 3)), κ_1 is the curvature of the lower crack arm.

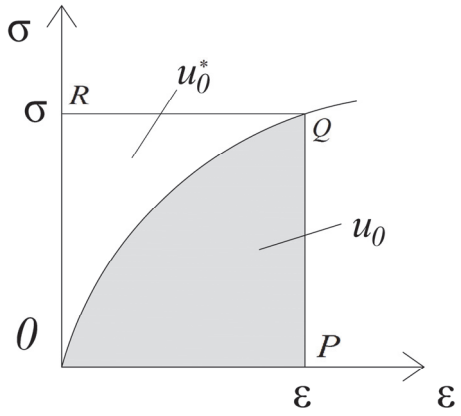

Figure 4: Schematic of a non-linear stress-strain curve (u_0 and u_0^* are the strain energy density and the complementary strain energy density, respectively).

The following equilibrium equations of the lower crack arm cross-section (Fig. 3) are used in order to determine z_{1n_1} and κ_1:

$$N_1 = \int_{-\frac{h_1}{2}}^{\frac{h_1}{2}} \left(\int_{-\frac{b}{2}}^{\frac{b}{2}} \sigma dy_1 \right) dz_1 \tag{13}$$

$$M_{y_1} = \int_{-\frac{h_1}{2}}^{\frac{h_1}{2}} \left(\int_{-\frac{b}{2}}^{\frac{b}{2}} \sigma z_1 dy_1 \right) dz_1 \tag{14}$$

where N_1 and M_{y_1} are the axial force and the bending moment, respectively. It is obvious that

$$N_1 = 0\,,\ M_{y_1} = M_y \tag{15}$$

By using (2), the distribution of material property, *B*, in the lower crack arm cross-section is written as

$$B = B_0 + \frac{4y_1^2}{b^2}B_1 + \frac{\left(r + z_1\right)^2}{b^2}B_2 \tag{16}$$

where

$$-\frac{b}{2} \le y_1 \le \frac{b}{2},\ -h_1/2 \le z_1 \le h_1/2\,,\ r = h - \frac{h_1}{2}. \tag{17}$$

By substituting of (1), (12) and (16) in (13) and (14), one derives

$$N_1=\left[\frac{B_0 b\kappa_1^m}{m+1}+\frac{B_1 b\kappa_1^m}{3(m+1)}+\frac{B_2 br^2\kappa_1^m}{h^2(m+1)}\right]\left(\eta_1^{m+1}-\eta_2^{m+1}\right)+$$
$$+\frac{2B_2 br\kappa_1^m}{h^2}\left[\frac{1}{m+2}\left(\eta_1^{m+2}-\eta_2^{m+2}\right)+\frac{z_{1n_1}}{m+1}\left(\eta_1^{m+1}-\eta_2^{m+1}\right)\right]+ \quad (18)$$
$$+\frac{B_2 b\kappa_1^m q}{h^2}\left[\frac{1}{f+3q}\left(\eta_1^{\frac{f+3q}{q}}-\eta_2^{\frac{f+3q}{q}}\right)+\frac{2z_{1n_1}}{f+2q}\left(\eta_1^{\frac{f+2q}{q}}-\eta_2^{\frac{f+2q}{q}}\right)+\right.$$
$$\left.+\frac{z_{1n_1}^2}{f+q}\left(\eta_1^{\frac{f+q}{q}}-\eta_2^{\frac{f+q}{q}}\right)\right]$$

$$M_{y1}=\left(B_0 b\kappa_1^m+\frac{B_1 b\kappa_1^m}{3}+\frac{B_2 br^2\kappa_1^m}{h^2}\right)\left[\frac{1}{m+2}\left(\eta_1^{m+2}-\eta_2^{m+2}\right)+\right.$$
$$\left.\frac{z_{1n_1}}{m+1}\left(\eta_1^{m+1}-\eta_2^{m+1}\right)\right]+\frac{2B_2 br\kappa_1^m q}{h^2}\left[\frac{1}{f+3q}\left(\eta_1^{\frac{f+3q}{q}}-\eta_2^{\frac{f+3q}{q}}\right)+\right.$$
$$\left.\frac{2z_{1n_1}}{f+2q}\left(\eta_1^{\frac{f+2q}{q}}-\eta_2^{\frac{f+2q}{q}}\right)+\frac{z_{1n_1}^2}{f+q}\left(\eta_1^{\frac{f+q}{q}}-\eta_2^{\frac{f+q}{q}}\right)\right]+ \quad (19)$$
$$+\frac{B_2 b\kappa_1^m q}{h^2}\left[\frac{1}{f+4q}\left(\eta_1^{\frac{f+4q}{q}}-\eta_2^{\frac{f+4q}{q}}\right)+\frac{3z_{1n_1}}{f+3q}\left(\eta_1^{\frac{f+3q}{q}}-\eta_2^{\frac{f+3q}{q}}\right)+\right.$$
$$\left.+\frac{3z_{1n_1}^2}{f+2q}\left(\eta_1^{\frac{f+2q}{q}}-\eta_2^{\frac{f+2q}{q}}\right)+\frac{z_{1n_1}^3}{f+q}\left(\eta_1^{\frac{f+q}{q}}-\eta_2^{\frac{f+q}{q}}\right)\right]$$

where $\eta_1=h_1/2-z_{1n_1}$, $\eta_2=-h_1/2-z_{1n_1}$ and $f/q=m$ (f and q are positive integers). In (19), N_1 and M_{y1} are determined by (15).

It is obvious that at m=1 the non-linear stress-strain relation (1) transforms into the Hooke's law, assuming that B=E (here E is the modulus of elasticity). This means that at m=1 Eq. (19) should transform into the formula for curvature of linear-elastic beam. Indeed, at m=1, $B_0=E$ and $B_1=B_2=0$ Eq. (19) yields

$$\kappa_1=\frac{12M_{y1}}{Ebh_1^3} \quad (20)$$

which is exact match of the formula for curvature of a linear-elastic homogeneous beam of width, b, and height, h_1.

Eqs. (18), and (19) should be solved with respect to z_{1n_1} and κ_1 by using the MatLab computer program.

By substituting of (12) and (16) in (11) the distribution of complementary strain energy density in the lower crack arm is written as

$$u_{0L}^*=\left[B_0+\frac{4y_1^2}{h^2}B_1+\frac{(r+z_1)^2}{h^2}B_2\right]\frac{m\left(z_1-z_{1n_1}\right)^{m+1}\kappa_1^{m+1}}{m+1} \quad (21)$$

Formula (21) can also be applied to obtain the distribution of complimentary strain energy density, u_{0U}^{*}, in the un-cracked beam portion. For this purpose, r, y_1, z_1, z_{1n_1} and κ_1 have to be replaced with 0, y_2, z_2, z_{2n_2} and κ_2, respectively (z_{2n_2} is the neutral axis coordinate of the cross-section of un-cracked beam portion, κ_2 is the curvature of un-cracked beam portion). The quantities, z_{2n_2} and κ_2, can be determined from Eqs. (18) and (19). For this purpose, r, z_{1n_1}, h_1 and κ_1 have to be replaced with 0, z_{2n_2}, $2h$ and κ_2, respectively.

Finally, by substituting of u_{0L}^{*}, u_{0U}^{*} and (8) in (7), one derives

$$
\begin{aligned}
G=&\frac{m\kappa_1^{m+1}}{b(m+1)}\left\{\left[\frac{B_0 b}{m_u+1}+\frac{B_1 b}{3(m_u+1)}+\frac{B_2 b r^2}{h^2(m_u+1)}\right]\left(\eta_1^{m_u+1}-\eta_2^{m_u+1}\right)+\right.\\
&+\frac{2B_2 b r}{h^2}\left[\frac{1}{m_u+2}\left(\eta_1^{m_u+2}-\eta_2^{m_u+2}\right)+\frac{z_{1n_1}}{m_u+1}\left(\eta_1^{m_u+1}-\eta_2^{m_u+1}\right)\right]+\\
&+\frac{B_2 b q_u}{h^2}\left[\frac{1}{f_u+3q_u}\left(\eta_1^{\frac{f_u+3q_u}{q_u}}-\eta_2^{\frac{f_u+3q_u}{q_u}}\right)+\frac{2z_{1n_1}}{f_u+2q_u}\left(\eta_1^{\frac{f_u+2q_u}{q_u}}-\eta_2^{\frac{f_u+2q_u}{q_u}}\right)+\right.\\
&\left.\left.+\frac{z_{1n_1}^2}{f_u+q_u}\left(\eta_1^{\frac{f_u+q_u}{q}}-\eta_2^{\frac{f_u+q_u}{q_u}}\right)\right]\right\}-\\
&-\frac{m\kappa_2^{m+1}}{b(m+1)}\left\{\left[\frac{B_0 b}{m_u+1}+\frac{B_1 b}{3(m_u+1)}\right]\left(\eta_{1u}^{m_u+1}-\eta_{2u}^{m_u+1}\right)+\right.\\
&+\frac{B_2 b q_u}{h^2}\left[\frac{1}{f_u+3q_u}\left(\eta_{1u}^{\frac{f_u+3q_u}{q_u}}-\eta_{2u}^{\frac{f_u+3q_u}{q_u}}\right)+\frac{2z_{2n_2}}{f_u+2q_u}\left(\eta_{1u}^{\frac{f_u+2q_u}{q_u}}-\eta_{2u}^{\frac{f_u+2q_u}{q_u}}\right)+\right.\\
&\left.\left.\left.+\frac{z_{2n_2}^2}{f_u+q_u}\left(\eta_{1u}^{\frac{f_u+q_u}{q}}-\eta_{2u}^{\frac{f_u+q_u}{q_u}}\right)\right]\right\}
\end{aligned}
\tag{22}
$$

where $m_u=m+1$, $f_u/q_u=m_u$ (f_u and q_u are positive integers), $\eta_{1u}=h-z_{2n_2}$ and $\eta_{2u}=-h-z_{2n_2}$.

Formula (22) calculates the strain energy release rate in the beam configuration shown in Fig. 1 when the beam mechanical behavior and the material gradient are described by formulae (1) and (2), respectively. It should be noted that at m=1, $B_0=E$, $B_1=B_2=0$ and $h_1=h$ formula (22) yields

$$
G=\frac{21M_y^2}{4Eb^2h^3} \tag{23}
$$

which is exact match of the expression for the strain energy release rate when the beam considered is linear-elastic and homogeneous [26].

In order to verify (22), the fracture is analyzed also by using the *J*-integral written as [27]

$$
J=\int_{\Gamma}\left[u_0\cos\alpha-\left(p_x\frac{\partial u}{\partial x}+p_y\frac{\partial v}{\partial x}\right)\right]ds \tag{24}
$$

where Γ is a contour of integration going from the lower crack face to the upper crack face in the counter clockwise direction, u_0 is the strain energy density, α is the angle between the outwards normal vector to the contour of integration and the crack direction, p_x and p_y are the components of stress vector, u and v are the components of displacement vector with respect to the crack tip coordinate system xy (x is directed along the crack), ds is a differential element along the contour.

The J-integral is solved by using an integration contour, Γ, that coincides with the beam contour (Fig. 1). It is obvious that the J-integral value is non-zero only in segments Γ_1 and Γ_2 of the integration contour. Therefore, the J-integral solution is written as

$$J = J_{\Gamma_1} + J_{\Gamma_2} \tag{25}$$

where J_{Γ_1} and J_{Γ_2} are the J-integral values in segments Γ_1 and Γ_2, respectively (Γ_1 and Γ_2 coincide with the free end of lower crack arm and the clamping, respectively).

The components of J-integral in segment, Γ_1, of the integration contour are written as (Fig. 3)

$$p_x = -\sigma = -B\varepsilon^m, \; p_y = 0 \tag{26}$$

$$ds = dz_1, \; \cos\alpha = -1 \tag{27}$$

where z_1 varies in the interval $[-h_1/2, \; h_1/2]$.

Partial derivative, $\partial u / \partial x$, in (24) is found as

$$\frac{\partial u}{\partial x} = \varepsilon = \left(z_1 - z_{1n_1}\right)\kappa_1 \tag{28}$$

where z_{1n_1} and κ_1 are obtained from Eqs. (18) and (19). The strain energy density is calculated by substituting of (1) in (10)

$$u_0 = \frac{B\varepsilon^{m+1}}{m+1} \tag{29}$$

By substituting of (1), (12), (16), (26), (27), (28) and (29) in (24) and integrating in boundaries from $-h_1/2$ to $h_1/2$, one derives

$$\begin{aligned} J_{\Gamma_1} = {} & \frac{m\kappa_1^{m+1}}{(m+1)}\left\{ \left[\frac{B_0}{m_u+1} + \frac{4\,y_1^2 B_1}{b^2(m_u+1)} + \frac{B_2 r^2}{b^2(m_u+1)} \right]\left(\eta_1^{m_u+1} - \eta_2^{m_u+1}\right) + \right. \\ & + \frac{2B_2 r}{b^2}\left[\frac{1}{m_u+2}\left(\eta_1^{m_u+2} - \eta_2^{m_u+2}\right) + \frac{z_{1n_1}}{m_u+1}\left(\eta_1^{m_u+1} - \eta_2^{m_u+1}\right) \right] + \\ & + \frac{B_2 q_u}{b^2}\left[\frac{1}{f_u+3q_u}\left(\eta_1^{\frac{f_u+3q_u}{q_u}} - \eta_2^{\frac{f_u+3q_u}{q_u}} \right) + \frac{2z_{1n_1}}{f_u+2q_u}\left(\eta_1^{\frac{f_u+2q_u}{q_u}} - \eta_2^{\frac{f_u+2q_u}{q_u}} \right) + \right. \\ & \left. \left. + \frac{z_{1n_1}^2}{f_u+q_u}\left(\eta_1^{\frac{f_u+q_u}{q}} - \eta_2^{\frac{f_u+q_u}{q_u}} \right) \right] \right\} \end{aligned} \tag{30}$$

where y_1 varies in the interval $\left[-b/2,\, b/2\right]$.

The *J*-integral solution in segment, Γ_2, of the integration contour (Fig. 1) can be determined by (30). For this purpose, r, z_{1n_1}, η_1, η_2 and κ_1 have to be replaced with 0, z_{2n_2}, η_{1u}, η_{2u} and κ_2, respectively. Besides, the sign of (30) must be set to „minus" because the integration contour is directed upwards in segment, Γ_2.

The *J*-integral final solution is found by substituting of J_{Γ_1} and J_{Γ_2} in (25)

$$
\begin{aligned}
J=&\frac{m\kappa_1^{m+1}}{(m+1)}\left\{\left[\frac{B_0}{m_u+1}+\frac{4y_1^2B_1}{b^2(m_u+1)}+\frac{B_2r^2}{b^2(m_u+1)}\right]\left(\eta_1^{m_u+1}-\eta_2^{m_u+1}\right)+\right.\\
&+\frac{2B_2r}{b^2}\left[\frac{1}{m_u+2}\left(\eta_1^{m_u+2}-\eta_2^{m_u+2}\right)+\frac{z_{1n_1}}{m_u+1}\left(\eta_1^{m_u+1}-\eta_2^{m_u+1}\right)\right]+\\
&+\frac{B_2q_u}{b^2}\left[\frac{1}{f_u+3q_u}\left(\eta_1^{\frac{f_u+3q_u}{q_u}}-\eta_2^{\frac{f_u+3q_u}{q_u}}\right)+\frac{2z_{1n_1}}{f_u+2q_u}\left(\eta_1^{\frac{f_u+2q_u}{q_u}}-\eta_2^{\frac{f_u+2q_u}{q_u}}\right)+\right.\\
&\left.\left.+\frac{z_{1n_1}^2}{f_u+q_u}\left(\eta_1^{\frac{f_u+q_u}{q}}-\eta_2^{\frac{f_u+q_u}{q_u}}\right)\right]\right\}-\\
&-\frac{m\kappa_2^{m+1}}{(m+1)}\left\{\left[\frac{B_0}{m_u+1}+\frac{4y_1^2B_1}{b^2(m_u+1)}\right]\left(\eta_{1u}^{m_u+1}-\eta_{2u}^{m_u+1}\right)+\right.\\
&+\frac{B_2q_u}{b^2}\left[\frac{1}{f_u+3q_u}\left(\eta_{1u}^{\frac{f_u+3q_u}{q_u}}-\eta_{2u}^{\frac{f_u+3q_u}{q_u}}\right)+\frac{2z_{2n_2}}{f_u+2q_u}\left(\eta_{1u}^{\frac{f_u+2q_u}{q_u}}-\eta_{2u}^{\frac{f_u+2q_u}{q_u}}\right)+\right.\\
&\left.\left.\left.+\frac{z_{2n_2}^2}{f_u+q_u}\left(\eta_{1u}^{\frac{f_u+q_u}{q}}-\eta_{2u}^{\frac{f_u+q_u}{q_u}}\right)\right]\right\}
\end{aligned}
\tag{31}
$$

Formula (31) describes the distribution of the *J*-integral value along the crack front. The average value of the *J*-integral along the crack front is written as

$$
J_{AV}=\frac{1}{b}\int_{-\frac{b}{2}}^{\frac{b}{2}}J\,dy_1 \tag{32}
$$

It should be noted that the *J*-integral solution derived by substituting of (31) in (32) is exact match of the strain energy release rate (22). This fact verifies the fracture analysis developed in the present paper.

RESULTS

The distribution of *J*-integral value along the crack front is analyzed. For this purpose, calculations are performed by using formula (31). It is assumed that b=0.020 m, h=0.004 m, m=0.7, f=7, q=10, $m_u=1.7$, $f_u=17$, $q_u=10$ and $M_y=20$ Nm.

The *J*-integral value is presented in non-dimensional form by using the formula, $J_N=J/(B_0b)$. The material gradient along the beam width is characterized by B_1/B_0 ratio. Fig. 5 shows the distribution of the *J*-integral value in non-

dimensional form along the crack front for two B_1 / B_0 ratios at $h_1 / 2h = 0.75$ and $B_2 / B_0 = 2$. Only the right-hand half of the crack front is shown in Fig. 5 since the distribution is symmetrical with respect to the crack front centre. The horizontal axis is defined such that $2y_1 / b = 0.0$ is in the crack front centre. Thus, $2y_1 / b = 1.0$ is in the right-hand lateral surface of the beam. One can observe in Fig. 5 that for $B_1 / B_0 = 1.2$, the *J*-integral value is maximum in the crack front centre and decreases towards the right-hand lateral surface (this is due to the fact that for $B_1 / B_0 = 1.2$ the material property, *B*, is minimum in the crack front centre and increases towards the beam lateral surfaces). Fig. 5 shows that for $B_1 / B_0 = -0.4$, the *J*-integral value increases from its minimum in the crack front centre towards the right-hand lateral surface of the beam.

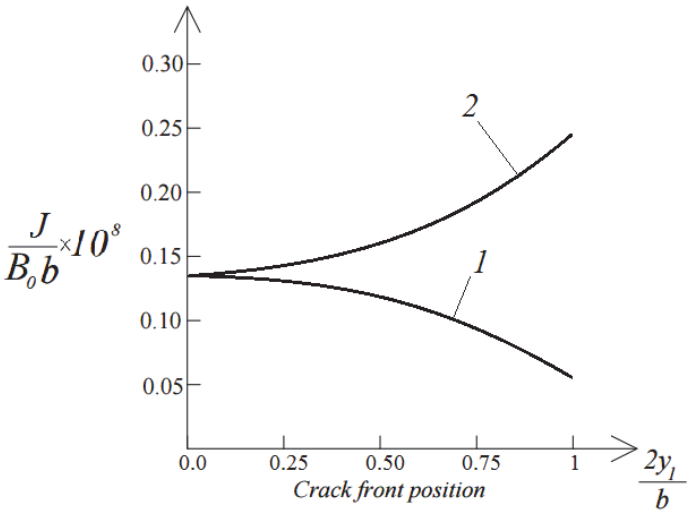

Figure 5: The distribution of the *J*-integral value in non-dimensional form along the crack front (curve *1* - at $B_1 / B_0 = 1.2$, curve *2* – at $B_1 / B_0 = -0.4$).

The effects of the material gradient and the crack location on the strain energy release rate are evaluated too. For this purpose, calculations of the strain energy release rate are carried-out by using formula (22). The strain energy release rate is presented in non-dimensional form by using the formula, $G_N = G / (B_0 b)$.

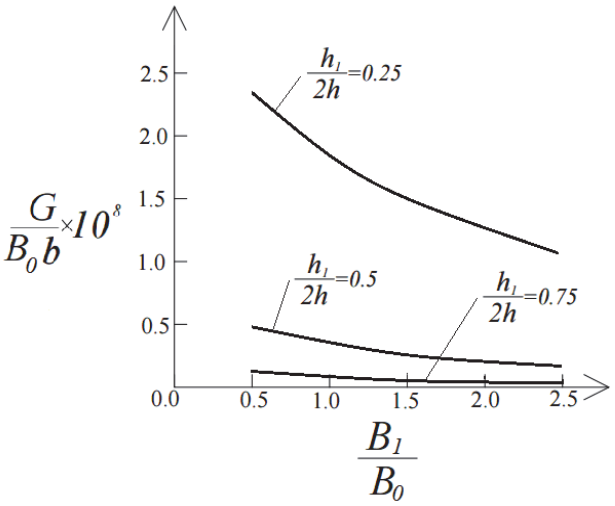

Figure 6: The strain energy release rate in non-dimensional form plotted against B_1 / B_0 ratio at three $h_1 / 2h$ ratios.

The crack location along the height of the beam cross-section is characterized by $h_1 / 2h$ ratio. In the calculations, B_0 is kept constant. Therefore, B_1 is varied in order to generate various B_1 / B_0 ratios. The strain energy release rate in non-dimensional form is plotted against B_1 / B_0 ratio at three $h_1 / 2h$ ratios and $B_2 / B_0 = 2.0$ in Fig. 6. The curves in Fig. 6 indicate that the strain energy release rate decreases with increasing of $h_1 / 2h$ ratio. This finding is attributed to the increase of the lower crack arm stiffness. It can be observed also in Fig. 6 that the strain energy release rate decreases with increasing of B_1 / B_0 ratio.

The influence of non-linear behavior of the material on the fracture is also analyzed. For this purpose, the strain energy release rate in non-dimensional form is presented as a function of B_2 / B_0 ratio at $h_1 / 2h = 0.5$ and $B_1 / B_0 = 0.5$ in Fig. 7. It can be observed that the strain energy release rate decreases with increasing of B_2 / B_0 ratio (Fig. 7). The strain energy release rate obtained assuming linear-elastic behavior of the two-dimensional functionally graded material is also presented in Fig. 7 for comparison with the non-linear solution (the linear-elastic solution is derived by substituting of m=1 in formula (22)). The curves in Fig. 7 indicate that material non-linearity leads to increase of the strain energy release rate.

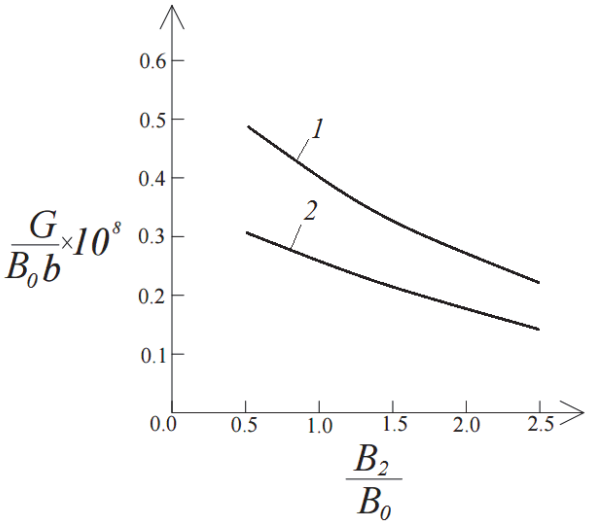

Figure 7: The strain energy release rate in non-dimensional form presented as a function of B_2 / B_0 ratio (curve *1* – at non-linear elastic behavior of material, curve *2* – at linear-elastic behavior of material).

CONCLUSIONS

The longitudinal fracture behavior of two-dimensional functionally graded cantilever beam that exhibits material non-linearity is investigated analytically. The beam is loaded by a bending moment applied at the free end of the lower crack arm. The fracture is studied in terms of the strain energy release rate. The beam mechanical behavior is described by using a power-law stress-strain relation. The material property, *B*, varies continuously in the beam cross-section according to a quadratic law.

The solution derived is applicable for longitudinal crack located arbitrary along the height of the beam cross-section. In order to verify the solution, the fracture is analyzed also by applying the *J*-integral approach. The distribution of the *J*-integral value along the crack front is investigated. The physical meanings of the dependence of the *J*-integral value on material gradient are discussed. The effects of material gradients and crack location along the beam height on the fracture behavior are also analyzed. The analysis revealed that the strain energy release rate decreases with increasing of the lower crack arm thickness. It is found also that the strain energy release rate decreases with increasing of B_1 / B_0 and B_2 / B_0 ratios. This finding is attributed to the increase of the beam stiffness. The influence of material non-linearity on the fracture is studied too. It is found that the material non-linearity leads to increase of the strain energy release rate. Therefore, non-linear behavior of the material has to be taken into account in fracture mechanics based safety design of structural members and components made of two-dimensional functionally graded materials. The results obtained in the

present study indicate that the longitudinal fracture in two-dimensional functionally graded beams with material non-linearity can be efficiently regulated in their design stage by employing appropriate material gradients.
Besides for the beam shown in Fig. 1, the analysis developed in the present paper can be applied to determine the strain energy release rate for longitudinal cracks in two-dimensional functionally graded non-linear elastic beam configurations loaded in pure bending (for instance, the double cantilever beam loaded with uneven bending moments, the four-point bending beam when the crack tip is located in middle beam portion which is loaded in pure bending). It should be noted that the approach developed in the present paper is applicable also for beam configurations loaded by a vertical load when the shear stresses can be neglected, i.e. when the span to height ratio of the beam is large.

ACKNOWLEDGMENTS

The present study was supported financially by the Research and Design Centre (CNIP) of the UACEG, Sofia (Contract BN – 198/2017).

REFERENCES

[1] Butcher, R.J., Rousseau, C.E., Tippur, H.V., A functionally graded particulate composite: Measurements and Failure Analysis, Acta Matererialia, 47 (1999) 259-268.
[2] Gasik, M.M., Functionally graded materials: bulk processing techniques, International Journal of Materials and Product Technology, 39 (1995) 20-29.
[3] Hirai, T., Chen, L., Recent and prospective development of functionally graded materials in Japan, Material Science Forum, 308-311 (1999) 509-514.
[4] Mortensen, A., Suresh, S., Functionally graded metals and metal-ceramic composites: Part 1 Processing, International Materials Review, 40 (1995) 239-265.
[5] Nemat-Allal, M.M., Ata, M.H., Bayoumi, M.R., Khair-Eldeen, W., Powder metallurgical fabrication and microstructural investigations of Aluminum/Steel functionally graded material, Materials Sciences and Applications, 2 (2011) 1708-1718.
[6] Neubrand, A., Rödel, J., Gradient materials: An overview of a novel concept, Zeit f Met, 88 (1997) 358-371.
[7] Suresh, S., Mortensen, A., Fundamentals of functionally graded materials, IOM Communications Ltd, London (1998).
[8] Tokova, L., Yasinskyy, A., Ma, C.-C, Effect of the layer inhomogeneity on the distribution of stresses and displacements in an elastic multilayer cylinder, Acta Mechanica, (2016) DOI: 10.1007/s00707-015-1519-8, 1 – 13.
[9] Tokovyy, Y., Ma, C.-C, Three-dimensional temperature and thermal stress analysis of an inhomogeneous layer, Journal of Thermal Stresses, 36 (2013) 790 – 808, DOI: 10.1080/01495739.2013.787853.
[10] Tokovyy, Y., Ma, C.-C, Axisymmetric stresses in an elastic radially inhomogeneous cylinder under length-varying loadings, ASME Journal of Applied Mechanics, 83 (2016), DOI: 10.1115/1.4034459.
[11] Uslu Uysal, M., Kremzer, M., Buckling behaviour of short cylindrical functionally gradient polymeric materials, Acta Physica Polonica A, 127 (2015) 1355-1357, DOI:10.12693/APhysPolA.127.1355.
[12] Uslu Uysal, M., Buckling behaviours of functionally graded polymeric thin-walled hemispherical shells, Steel and Composite Structures, An International Journal, 21 (2016) 849-862.
[13] Szekrenyes, A., Fracture analysis in the modified split-cantilever beam using the classical theories of strength of materials, Journal of Physics: Conference Series, 240 (2010) 012030.
[14] Szekrenyes, A., Vicente, W.M., Interlaminar fracture analysis in the GII-GIII plane using prestressed transparent composite beams, Composites Part A: Applied Science and Manufacturing, 43 (2012) 95-103.
[15] Szekrenyes, A., Semi-layerwise analysis of laminated plates with nonsingular delamination - The theorem of autocontinuity, Applied Mathematical Modelling, 40 (2016) 1344 – 1371.
[16] Bohidar, S.K., Sharma, R., Mishra, P.R., Functionally graded materials: A critical review, International Journal of Research, 1 (2014) 289-301.
[17] Erdogan, F., Fracture mechanics of functionally graded materials, Computational Engineering, 5 (1995) 753-770.
[18] Paulino, G.C., Fracture in functionally graded materials, Engineering Fracture Mechanics, 69 (2002) 1519-1530.

[19] Shi-Dong Pan, Ji-Cai Feng, Zhen-Gong Zhou, Wu-Lin-Zhi, Four parallel non-symmetric Mode –III cracks with different lengths in a functionally graded material plane, Strength, Fracture and Complexity: an International Journal, 5 (2009) 143-166.
[20] Tilbrook, M.T., Moon, R.J., Hoffman, M., Crack propagation in graded composites, Composite Science and Technology, 65 (2005) 201-220.
[21] Upadhyay, A.K., Simha, K.R.Y., Equivalent homogeneous variable depth beams for cracked FGM beams; compliance approach, International Journal of Fracture, 144 (2007) 209-213.
[22] Uslu Uysal, M., Güven, U., A bonded plate having orthotropic inclusion in adhesive layer under in-plane shear loading, The Journal of Adhesion, 92 (2016) 214-235, DOI:10.1080/00218464.2015.1019064.
[23] Petrov, V.V., Non-linear incremental structural mechanics, Infra-Injeneria, M. (2014).
[24] Tsukamoto, H., Mechanical properties of zirconia – titanium composites, International Journal of Materials Science and Applications, 3 (2014) 260-267.
[25] Lubliner, J., Plasticity theory (Revised edition), University of California, Berkeley, CA (2006).
[26] Hutchinson, W., Suo, Z., Mixed mode cracking in layered materials, Advances in Applied Mechanic, 64 (1992) 804–810.
[27] Broek, D., Elementary engineering fracture mechanics, Springer (1986).